A Nerve-Fibroblast Axis in Mammalian Lung Fibrosis

Genta Ishikawa[1#], Xueyan Peng[1#], John McGovern[1], Alexander Ghincea[1], Samuel Woo[1], Daisuke Okuno[1], Sheeline Yu[1], Chris J. Lee[1], Angela Liu[1], Tina Saber[1], Buqu Hu[1], Ying Sun[1], Huanxing Sun[1], Karam Al Jumaily[1], Carol Feghali-Bostwick[2], Tomokazu S. Sumida[3], Maor Sauler[1], Changwan Ryu[1], and Erica L. Herzog[1,4]*

[#]authors contributed equally to this work

*to whom correspondence should be addressed

[1]Department of Internal Medicine, Section of Pulmonary, Critical Care, and Sleep Medicine, School of Medicine, Yale University, New Haven, CT, USA
[2]Department of Medicine, Division of Rheumatology and Immunology, Medical University of South Carolina, SC, USA
[3]Department of Neurology, School of Medicine, Yale University, New Haven, CT, USA
[4]Department of Pathology, School of Medicine, Yale University, New Haven, CT, USA

Corresponding author

Erica L. Herzog, M.D., Ph.D.
300 Cedar Street
The Anlyan Center S441
New Haven, CT 06520-8057
Email: erica.herzog@yale.edu
Phone 203 737 4612
Fax 203 785 3826
ORCiD: 0000-0002-7508-8575

AUTHOR CONTRIBUTIONS

GI conceptualized the project, administered its execution, secured funding, conducted the investigation, interpreted the data, and contributed to both writing and editing the manuscript. XP, JM, AG, SW, DO, SY, CJL, AL, TS, BH, and YS carried out the investigation and data analysis. KIJ administered the project. CFB provided resources. TSS and MS contributed to project conceptualization. HS provided supervision. CR provided supervision, resources, administered the project, and acquired funding alongside ELH, who contributed similarly in these areas. ELH also interpreted the data, assisted in conceptualization and participated as the corresponding author in writing and editing the manuscript. All authors were involved in preparing the manuscript and approved the final version for submission.

FUNDING

GI was supported by T32HL007778-25, a Scholar Award from the Pulmonary Fibrosis Foundation, Wit Family Distinguished Scholar in Inflammation Science, and Yale Physician Scientist Development Award (UL1 TR001863). HS was supported by U.S. Department of Defense (DOD) Award W81XWH-20-1-0157. CFB was supported by K24AR060297. MS was supported by R01HL155948. CR was supported by K08HL151970-01 and Boehringer-Ingelheim Discovery Award. ELH was supported by R01HL152677 and R01HL163984, the Gabriel and Alma Elias Research Fund, and the Greenfield Foundation. The content is solely the responsibility of the authors and does not necessarily represent the official views of the National Institutes of Health or the Department of Defense.

Word Count 4,738 words (Abstract Count 149 words)

ABSTRACT

Tissue fibrosis contributes to pathology in vital organs including the lung. Curative therapies are scant. Myofibroblasts, pivotal effector cells in tissue fibrosis, accumulate via incompletely understood interactions with their microenvironment. In an investigative platform grounded in experimental lung biology, we find that sympathetic innervation stimulates fibrotic remodeling via noradrenergic α1-adrenergic receptor engagement in myofibroblasts. We demonstrate the anti-fibrotic potential of targeted sympathetic denervation and pharmacological disruption of noradrenergic neurotransmitter functions mediated by α1-adrenoreceptors (α1-ARs). Using the α1-adrenoreceptor subtype D as a representative α1-AR, we discover direct noradrenergic input from sympathetic nerves to lung myofibroblasts utilizing established mouse models, genetic denervation, pharmacologic interventions, a newly invented transgenic mouse line, advanced tissue mimetics, and samples from patients with diverse forms of pulmonary fibrosis. The discovery of this previously unappreciated nerve-fibroblast axis in the lung demonstrates the crucial contribution of nerves to tissue repair and heralds a novel paradigm in fibrosis research.

Keywords

α1-adrenoreceptor, fibrosis, myofibroblast, noradrenaline, sympathetic nerve

INTRODUCTION

Tissue fibrosis arising from ineffective wound healing is implicated in human pathologies affecting critical organs such as the lung [1], heart [2], liver [3], kidney [4], and skin [5]. The process is currently viewed as irreversible and contributes to upwards of 45% deaths in the industrialized world [6]. While in the last two decades progress has been made with the development of modestly effective therapies for pulmonary fibrosis [7, 8], curative treatments are lacking and the disease burden remains high. This shortcoming results in part from limited understanding of cellular and molecular mechanisms contributing to pathology, and presents an imperative for the discovery of new opportunities for research and therapeutic innovation.

Successful wound repair requires the expansion of activated myofibroblasts that receive and respond to microenvironmental signals by contracting the wound bed and producing extracellular matrix [9]. From a tissue perspective, repair resolution and functional restoration require that myofibroblast programming shift from activated expansion to quiescent regression [10]. Because myofibroblast persistence is a hallmark of fibrotic diseases affecting the lung and other organs [11], fibrosis has evolved to be viewed as an unrelenting form of maladaptive repair and regenerative failure. Interestingly, while the mechanisms driving myofibroblast activation have been well studied [10], less is known about myofibroblast persistence. This pathology is proposed to involve emergent effector cell populations that experience perturbations in such critical fate decisions as proliferation and death. The discovery of fundamental yet intervenable processes governing this biology would be a major advance for the treatment of fibrosis affecting the lung and other organs.

The nervous system controls organismal homeostasis in health and disease and is increasingly implicated in tissue level injury and remodeling responses [12-18]. In the lung, autonomic input controls the physiology of airways, blood vessels, and secretory glands but there is only limited information regarding the role of local innervation in disease processes. Several groups,

including our own, have studied autonomic and sensory nerves in conditions of inflammatory remodeling but most of these studies have focused on immune cell activation, airway disorders, and/or host defense [14, 19-21]. Far less is known about the contribution of lung innervation to effector cells such as myofibroblasts under conditions of repair and pathologic remodeling affecting alveoli, which are critical gas exchange regions in the lung. While alveolar myofibroblasts have been recently shown to require autonomic nerve input for proper lung development [22], an analogous relationship between nerves and the alveolar myofibroblasts that arise during fibrosis is highly plausible but has not been shown. The discovery that the lung's autonomic nerve supply directs alveolar myofibroblast function would substantially advance the pathobiological understanding of pulmonary fibrosis and provide numerous new targets for therapeutic intervention.

Using an experimental platform comprised of mouse genetics, pharmacology, advanced human lung mimetics, cell-based assays, and specimens from patients with pulmonary fibrosis, we report a new role for autonomic innervation, specifically sympathetic nerves, in directing alveolar myofibroblast biology during pulmonary fibrosis. This work provides new opportunities for therapeutic development and illuminates a previously unrecognized process by which two discrete organ systems – the autonomic nervous system and the lungs – form a functional axis during repair and fibrosis in higher organisms.

METHODS

Study approval

All animal experiments were approval by the Yale University Institutional Animal Care and Use Committee (IACUC) and were conducted in compliance with the guidelines outlined in the Guide for the Care and Use of Laboratory Animals [23]. Deidentified control, idiopathic pulmonary

fibrosis (IPF), and systemic sclerosis-related interstitial lung disease (SSc-ILD) lung tissues were obtained at the time of lung transplantation under a human subjects protocol approved by the University of Pittsburgh IRB or from deidentified autopsy samples obtained from Yale Pathology.

Animals

Wild-type male and female C57BL/6J mice obtained from The Jackson Laboratory (Bar Harbor, ME) were used between 8 to 12 weeks of age. Transgenic mice used in this study included B6.Cg-*7630403G23Rik*$^{Tg(Th\text{-}cre)1Tmd}$/J (*Th-Cre*), B6(Cg)-Tg(Acta2-cre/ERT2)1Ikal/J (*Acta2-CreERT2*), B6.129P2-Lyz2$^{tm1(cre)Ifo}$/J (*LysMCre*), B6.129P2(Cg)-*Slc6a2*$^{tm1.1Hhg}$/J (*Slc6a2*$^{-/-}$), and *B6.Cg-Gt(ROSA)26Sor*$^{tm6(CAG\text{-}ZsGreen1)Hze}$*/J* (*ROSA26R*$^{Zs/+}$) mice and were all purchased from The Jackson Laboratory (Bar Harbor, ME). The B6.129P2(SJL)-*Ntrk1*^{tm1Ddg}/J (*Ntrk1*$^{f/f}$) mice, created and provided by Dr. Donald Ginty, were also purchased from Jackson Laboratories under an MTA from Johns Hopkins University. B6/JGpt-*Adra1dem1Cflox*/Gpt (*Adra1d*$^{f/f}$) mice were generated on a fee for service basis by GemPharmatech Co., Ltd, Nanjing, China. Briefly, the *Adra1d* gene was modified by utilizing CRISPR/Cas9 technology. The single-guide RNA (sgRNA) was transcribed *in vitro*, and a donor vector was constructed. The Cas9 enzyme, sgRNA, and a donor vector—which flanked the protein-coding regions of exons 1 and 2 with loxP sites—were microinjected into the fertilized eggs of C57BL/6J mice. These fertilized eggs were then transplanted to produce F0 generation mice, which were confirmed to carry the modification through polymerase chain reaction (PCR) and sequencing. When needed, mice were backcrossed for > 10 generations onto the C57BL/6J background.

Inhaled bleomycin administration

Oropharyngeal bleomycin administration (2.0U/kg, Mckesson, 63323013610) was performed as previously reported [12, 14]. Control and treatment groups were maintained under identical

conditions. Specimens from animals that did not survive to the prespecified endpoints were excluded from analysis.

Administration of experimental agents

Mice were allocated into groups that received daily intraperitoneal injections of PBS control or experimental agents from days 5-13 post bleomycin. Experimental agents included terazosin (1 mg/kg, U.S. Pharmacopeia, 1643452), atenolol (1 mg/kg, Sigma-Aldrich, A7655), ICI118,551 (1 mg/kg, Sigma-Aldrich, I127), or nisoxetine (3 or 10 mg/kg, MilliporeSigma, 57754-86). An additional cohort received PBS or terazosin (1 or 10 mg/kg, U.S. Pharmacopeia, 1643452) via daily oral gavage on the same schedule.

Tamoxifen Administration

Depending on the deletion schedule, mice received injections of tamoxifen (2 mg per day for either 5 or 7 days, Sigma-Aldrich, T5648) or an equivalent volume of corn oil as a vehicle control. Thereafter, mice either received immediate bleomycin injections or were allowed a 7-day rest period before bleomycin administration.

Sacrifice and lung harvest

Fourteen days following bleomycin, mice underwent terminal anesthesia, bronchoalveolar lavage (BAL), median sternotomy, right heart perfusion with 1x PBS, and *en bloc* lung resection [12, 24].

Determination of noradrenaline concentrations

Noradrenaline concentrations were quantified in plasma and BAL fluid using high-sensitivity ELISA kits (DLD Diagnostika, GMBH, NOU39-K01) as previously reported [12, 14].

Collagen quantification

Lungs were snap frozen in liquid nitrogen and stored at −80°C until quantification of lung collagen using the Sircol Collagen Assay (Biocolor Ltd., S1000) or Hydroxyproline Assay (QuickZyme Biosciences, QZBHYPRO5) as previously reported [12, 14, 24].

Flow cytometry analysis on digested lung tissues

Flow cytometry analysis was carried out using an LSRII flow cytometer (BD Biosciences, Franklin Lakes, NJ) on lung tissue suspensions from euthanized mice. The lungs were first perfused with 1x PBS, then harvested, minced, and digested in 1x PBS containing 150 µg/ml collagenase (MilliporeSigma, C5138) and 20 U/ml DNase I (Roche, 04716728) for 1 hour at room temperature. The digestion was quenched with 1x PBS. Suspensions were filtered through a 40-µm cell strainer and centrifuged at 495 g for 10 minutes at 4°C. The supernatants were discarded, and the pellets were resuspended in 10 ml of 1x PBS for cell counting. After another round of centrifugation, cell pellets were resuspended in FACS buffer (1× PBS with 1% fetal bovine serum [FBS], 0.01% NaN3, and 1 mM EDTA) to a concentration of 1 x 10^6 cells/ml. For staining, 1 x 10^6 cells were incubated with a series of antibodies at specific dilutions in FACS buffer containing 10% normal goat serum (NGS) for 1 hour at 4°C. The staining panel included: rat anti-CD45 FITC (1:100, eBioscience, 11-0451-82), rat anti-CD45 PE (1:100, BD Biosciences, 553081), rat anti-CD45 PerCP (1:1000, eBioscience, 45-0451-82), rat anti-CD45 APC (1:100, eBioscience, 17-0451-82), rabbit anti-ADRA1D (1:100, Abcam, ab84402), rat anti-CD11b PE (1:200, BD Biosciences, 557397), Armenian hamster anti-CD11c PerCP-Cy5.5 (1:800, eBioscience, 45-0114-80), rat anti-F4/80 APC (1.5:100, Invitrogen, 17-4801-82), and mouse anti–α-SMA (1:250, intracellular staining, Abcam, ab7817). Secondary antibodies were used as necessary for detection of unconjugated primary antibodies. Following staining, cells were washed, filtered through a 40-µm cell strainer, and then subjected to data acquisition on the LSRII flow cytometer using FACSDiva software (BD Biosciences, Franklin Lakes, NJ). Data analysis was conducted using FlowJo software (BD Biosciences, Franklin Lakes, NJ),

182 employing gating strategies refined by control samples incubated without primary antibodies.
183 This approach ensured accurate identification of positive and negative cell populations.
184 ZsGreen-expressing cells were isolated from *Acta2-CreERT2 (ROSA26R$^{Zs/+}$); Adra1d$^{f/f}$* mice
185 through flow cytometry, specifically targeting cells that express α-SMA.

186 **Histologic analysis**

187 Resected left lungs were fixed in 10% formalin, embedded in paraffin, sectioned, and stained
188 with Masson's Trichrome [12].

189 **Human lung fibroblast culture**

190 MRC5 fibroblasts, normal human lung fibroblasts, and IPF fibroblasts were procured from ATCC
191 (Manassas, VA), Lonza (Allendale, NJ), and Asterand Bioscience (Detroit, MI), respectively.
192 Cells used at passages 5-10 were cultured to confluence in Dulbecco's Modified Eagle
193 Medium/10% Fetal Bovine Serum/1% penicillin-streptomycin. Approximately 400,000 cells were
194 seeded into each well of a 6-well plate. After 24 hours of serum deprivation, the cells were
195 exposed to various concentrations of noradrenaline (0, 5, 12.5, and 25 μM; Sigma-Aldrich,
196 A0937-5G) for 48 hours, with/without concurrent administration of terazosin (10 μM; Sigma-
197 Aldrich, T4680). After treatment, samples were collected for analysis.

198 **Precision cut lung slices**

199 Normal human precision-cut lung slices (PCLS) were purchased from the Institute for In Vitro
200 Sciences (Gaithersburg, MD). PCLS were rapidly thawed and transferred to an acclimation
201 medium, which consisted of DMEM/F12 (Thermo Fisher, 11320033), 0.2% Primocen®
202 (Invivogen, ANT-PM-1), 1% insulin-transferrin-selenium (Thermo Fisher, 41400045), 1%
203 Antibiotic Antimycotic solution (Millipore Sigma, A5955), 2 μM hydrocortisone (Millipore Sigma,
204 H0888), and 2-phospho-L-ascorbic acid trisodium salt (Millipore Sigma, 49752). Following three
205 days of culture in this medium, PCLS were transferred to a culture medium composed of DMEM

supplemented with 0.2% Primocen® and 1% insulin-transferrin-selenium for three days. Next, PCLS were cultured in the absence or presence of a pro-fibrotic media for five days consisting of the following: 5 ng/ml TGFβ (Bio-Techne Corporation, 240-GMP-010), 5 μM platelet-derived growth factor-AB (PDGF-AB, ThermoFisher, 100-00AB-10UG), 10 ng/ml tumor necrosis factor alpha (TNF-α, R&D Systems, 210-TA), and 5 μM lysophosphatidic acid (Cayman Chemical, 62215). PCLS were then treated in the absence or presence of 10 μM terazosin (U.S. Pharmacopeia, 1643452) for 24 hours. Subsequently, the PCLS were harvested and prepared either for RNA analysis using Qiazol or for histological examination.

Immunofluorescence analysis of mouse and human lung tissues

Immunofluorescence analysis for the detection of α1-adrenoreceptors (α1-AR), CD68, and αSMA in mouse and human lung sections utilized the following primary antibodies: rabbit anti-ADRA1A (1:100, Abcam, ab137123), rabbit anti-ADRA1B (1:250, Abcam, ab169523), rabbit anti-ADRA1D (1:250, Abcam, ab84402), rabbit anti-ADRA1D (1:250, LSBio, LS-A12-50), rat anti-CD68 (1:250, Invitrogen, 14-0681-82), and mouse anti–α-SMA (1:250, Abcam, ab7817). After primary antibody application, sections were subjected to secondary antibody detection and nuclei were counterstained with 4′,6-diamidino-2-phenylindole (DAPI). Human prostate tissues were employed as positive controls for the specificity of the anti-ADRA1D antibody. Negative controls included slides processed without primary antibodies. Imaging was performed using a Nikon Eclipse microscope (Nikon Corporation, Tokyo, Japan), equipped with coherent 488 and 561 nm lasers. Image capture was facilitated by an Andor iXON3 EMCCD detector, with NIS Elements AR software (Nikon Corporation, Tokyo, Japan) controlling the imaging process.

Immunofluorescence and imaging of lung nerves

Vibratome sectioning and immunofluorescence staining were utilized to ubiquitin carboxy-terminal hydrolase L1 (PGP9.5) and tyrosine hydroxylase (TH). The preparation of lung tissues

for vibratome sectioning adhered to established protocols [25]. Sections measuring 150 µm were blocked overnight at 4°C on a shaker in a solution of 5% normal goat serum (NGS) diluted in 0.5% Triton X-100 and 1× PBS (PBS-T). Following blocking, these sections were incubated with either a mouse anti-PGP9.5 (1:100, Abcam, ab8189) or a rabbit anti-TH antibody (1:100, Abcam, ab112) for three days at 4°C. After thorough rinsing with PBS-T, the sections were treated with Alexa Fluor 555–conjugated goat anti-rabbit IgG (1:500, Invitrogen, A10931) overnight at 4°C. Subsequent to four washes in PBS-T, the sections were mounted using DAPI-supplemented VECTASHIELD antifade mounting medium (Vector Laboratories, H1200). Maximum intensity projections of the stained sections were captured using an SP8 confocal laser microscope operated with Leica Application Suite X software (Leica Microsystems, IL).

BrdU Assay

Cultured fibroblasts were treated with 10 µg/ml BrdU (BOC Sciences, B2706-004257) for three hours at 37°C. After two washes with PBS, the cells were fixed with 4% paraformaldehyde (Thermo Fisher, J61899-AK) for 30 minutes at room temperature. Following fixation, the cells were rinsed with 0.3% Tris and 1.5% glycine in water for 15 minutes. The cells were then incubated with 2N HCl for 30 minutes at 37°C, followed by a wash with 0.1M boric acid for 1 minute. Subsequently, the cells were incubated in 1% FBS in PBS-T for 1 hour at room temperature. After this incubation, the cells were stained with rat anti-BrdU primary antibody (1:500, BioRad, MCA2483T) for one hour at room temperature. Following three washes with PBS-T, the cells underwent nuclear staining with propidium iodide (PI).

MTT assay

MRC5, normal human lung, and IPF fibroblasts underwent the 3-(4,5-Dimethylthiazol-2-yl)-2,5-diphenyltetrazolium bromide (MTT) assay (ThermoFisher Scientific, M6494) according to the manufacturer's protocol. Briefly, fibroblasts were labeled with 12 nM MTT, lysed with DMSO,

and analyzed at an absorbance of 570 nm using the Vmax Kinetic Microplate Reader with SoftMax Pro 5.4 software (Molecular Devices, Sunnyvale, CA).

RNA isolation and real time quantitative PCR

Total cellular RNA was extracted using the miRNeasy Mini-Kit (Qiagen, 217084) according to the manufacturer's protocol. This RNA was then reverse-transcribed using the Power SYBR™ Green RNA-to-CT™ 1-Step Kit (Applied Biosystems, 4389986). Subsequent analysis focused on the expression levels of *ACTA2* and *GAPDH* (human) and *Adra1d* and *Actb* (mouse) using specific primers for each gene on the ViiA 7 Real-Time PCR System (Thermo Fisher, Waltham, MA). Relative gene expression was quantified using the 2-delta Ct method, consistent with our methodologies [24].

Human primers were:

ACTA2-F: 5′ -GTGTTGCCCCTGAAGAGCAT -3′ ;

ACTA2-R: 5′ -GCTGGGACATTGAAAGTCTCA -3′ ;

GAPDH-F: 5′ -TGGAGAAGGCTGGGGCTCATTT-3′ ;

GAPDH-R: 5′ -TGGTGCAGGAGGCATTGCTGAT-3′ ;

Mouse primers were:

Actb-F: 5′ -GGCTGTATTCCCCTCCATCG-3′ ;

Actb-R: 5′ -CCAGTTGGTAACAATGCCATGT-3′ ;

Adra1d-F: 5′ -AATCTTGCTGCACTAGGGCTCT-3′ ;

Adra1d-R: 5′-CTAGTCATGTCAACAGGAGCTGGA-3′;

Graphics

Graphics were designed using BioRender.com (Toronto, Ontario, Canada).

Statistical Analyses

All data are presented as mean ± SEM or median ± IQR unless stated otherwise. Normally distributed data were compared using 1- or 2-tailed student's t test or ANOVA with Tukey's multiple comparisons test. Non-normally distributed data were compared using the nonparametric Mann-Whitney test or Kruskal-Wallis test with Dunn's multiple comparisons test. Statistical correlations were conducted using Spearman's Rank Correlation Coefficient. GraphPad Prism 9.0 (GraphPad Software, CA) was used for all these analyses. A p-value < 0.05 corrected for multiple testing considered significant.

RESULTS

Association of sympathetic nerves and myofibroblasts in fibrotic lungs

To study whether lung innervation directs pulmonary fibrosis, we employed a widely used bleomycin model [26]. This approach consistently induces fibrosis, as evidenced by trichrome staining of lung tissues (Figure 1A and B) and biochemical collagen measurements (Figure 1C). This fibrotic response is paralleled by accumulation of local but not circulating noradrenaline (Figure 1D and E) that may originate from the lung's sympathetic nerve supply. To more firmly illustrate this concept, we performed immunofluorescence detection and confocal reconstruction of ubiquitin carboxy-terminal hydrolase L1 (alias PGP9.5, a pan-neuronal marker) or tyrosine hydroxylase (TH, sympathetic nerve specific rate limiting enzyme in catecholamine synthesis). Uninjured mouse lungs demonstrated expected patterns of PGP9.5 and TH nerve presence in airways and blood vessels (Figures 1F and I). Notably, fibrotic lungs also contained these nerves, along with PGP9.5 and TH-positive nerve-like structures in alveolar regions populated

by α-SMA+ myofibroblasts (Figure 1G and J). The detection of noradrenaline and TH+ nerves alongside α-SMA+ myofibroblasts indicates a functional innervation unit, as evidenced by a positive correlation between both nerve types and these pivotal effector cells (Figure 1H and K). These observations imply that following injury, noradrenergic signals from sympathetic nerves interact with α-SMA+ myofibroblasts in the adult lung.

Bleomycin-induced fibrotic endpoints are mitigated in Th-Cre; Ntrk1$^{f/f}$ mouse lungs

Next, we asked whether sympathetic nerves are directly required for fibrosis. This inquiry aligns with the hypothesis that cells within fibrotic areas receive and respond to neurotransmitters released by nerves in their vicinity. Although there is some evidence suggesting a connection between sympathetic innervation and fibrosis in the lungs and other organs [12-18], the direct and definitive role of this relationship has yet to be established. Here we employed a well characterized genetic approach involving sympathetic nerve specific deletion of neurotrophic tyrosine kinase receptor type 1 (*Ntrk1*, also known as TrkA [27]). *Ntrk1* encodes the high affinity neurotrophin receptor for nerve growth factor, which is required for survival and innervation by sympathetic nerves [28, 29]. While *Ntrk1*'s roles in lung development [30] and host defense [31] have been explored, its involvement in pulmonary fibrosis has yet to be elucidated.

To investigate direct interactions between sympathetic nerves and their target cells in pulmonary fibrosis, we engineered mice with *Ntrk1* deletion confined to TH+ sympathetic nerves (*Th-Cre; Ntrk1$^{f/f}$*). After administering bleomycin, BAL noradrenaline was significantly suppressed in *Th-Cre; Ntrk1$^{f/f}$* mice, compared to their *Ntrk1$^{+/+}$* counterparts (Figure 1L). Notably, the lack of sympathetic innervation led to an approximate 20% reduction in collagen levels (Figure 1M) and an improved appearance of trichrome-stained tissues (Figure 1N and O). These results provide definitive evidence that sympathetic innervation plays a direct and functional role in experimentally induced pulmonary fibrosis.

Loss of function of noradrenaline receptors, but not transporter, mitigates bleomycin induced lung fibrosis

Sympathetic nerve derived noradrenaline may influence fibrosis through distinct mechanisms including neurotransmitter functions mediated by postsynaptic G-protein coupled receptors (GPCRs), and/or cellular perturbations driven by noradrenaline transporters such as solute carrier family 6 member 2 (Slc6a2, [32, 33]). To distinguish between these mechanisms, loss of function studies were conducted that probed noradrenaline's well-characterized receptors and transporters using robust pharmacological inhibitors. In studies targeting GPCRs, bleomycin-challenged mice received systemic administration of the α1-adrenoreceptor (α1-AR) antagonist terazosin (Figures 2A-D), the β1 receptor antagonist atenolol, and the β2 receptor antagonist ICI118,551 (Figures 2E-H). All interventions were sufficient to improve collagen measurements and histology, supporting a role for noradrenaline's neurotransmitter function via GPCRs in fibrosis. Conversely, fibrotic endpoints remained unchanged in noradrenaline transporter loss of function achieved through administration of nisoxetine, a specific inhibitor of Slc6a2 (Figures 2I-L), and genetic approaches in *Slc6a2*$^{-/-}$ mice (Figures 2M-O). These findings underscore the pivotal role of noradrenaline's GPCR-mediated neurotransmitter functions in experimentally induced fibrosis.

ADRA1D+ alveolar myofibroblasts accumulate in conditions of established fibrosis

β-adrenergic receptors are essential regulators of airway physiology and cardiac function, while under normal circumstances α1-adrenergic signaling does not possess such functions. Therefore, α1-ARs are an attractive target for the development of antifibrotic therapies. In line with this notion, the use of α1 blockers, but not β blockers, has been associated with improved clinical outcomes in human conditions of inflammatory fibrosis affecting the lung [12, 14, 34, 35]

and central nervous system [36-38]. However, the mechanisms underlying these benefits remain elusive.

The simplest explanation of our findings is that nerve-derived noradrenaline directly mediates the effector functions of α-SMA+ alveolar myofibroblasts through cell-autonomous mechanisms. This supposition requires the expression of one or more α1-AR on alveolar myofibroblasts in lesional lung tissue. Evidence supporting this concept was obtained when the lungs of bleomycin challenged mice showed time dependent enrichment of α-SMA+ fibroblasts expressing α1-adrenoreceptor subtype D (ADRA1D) that peaked at day 14 (Figures 3A-D, Figure S1). These findings were corroborated in deidentified human lung specimens, where the lungs of patients with two forms of pulmonary fibrosis contained large quantities of cells expressing ADRA1D (Figures 3E-H, Figure S2A and B), but not ADRA1A or ADRA1B (Figure S2C and D). Many of the emergent ADRA1D+ cells co-expressed α-SMA (Figures 3I-L). These findings show that α-SMA+ effector cells in fibrotic lungs from two species are poised to receive noradrenergic signals from sympathetic nerves via expression of ADRA1D.

Deletion of Adra1d in alveolar myofibroblasts mitigates experimentally induced lung fibrosis

Given the proximity of TH+ nerves to α-SMA+ cells, and the extensive detection of ADRA1D on α-SMA+ myofibroblasts in fibrotic alveoli, we surmised that ADRA1D expression in α-SMA+ cells facilitates the reception of fibrogenic noradrenergic signals in the lung. To test this hypothesis, we disrupted ADRA1D receptor function in myofibroblasts by creating a model of pan-myofibroblast *Adra1d* deletion. This goal was achieved by crossing mice with the tamoxifen-inducible *Acta2-CreERT2* promoter with a newly invented transgenic model in which *Adra1d* gene was floxed. This mouse line was created specifically for this project. Here, CRISPR-Cas9 technology was employed to insert loxP sites flanking exons 1 and 2 of the

Adra1d gene, creating the *Adra1d*$^{f/f}$ mouse line (Figure 4A). The *Acta2-CreERT2* mouse line has been extensively utilized in studies of fibrosis [39], vascular biology [40], and wound healing [41]. *Acta2-CreERT2; Adra1d*$^{f/f}$ mice were viable, fertile, and displayed no significant changes in lung appearance compared to their *Acta2-CreERT2; Adra1d*$^{+/+}$ littermates. Upon tamoxifen administration, these mice developed specific reduction in *Adra1d* expression within *Acta2*+ cells (Figure 4B and C).

Tamoxifen was administered according to a schedule designed to delete ADRA1D approximately 7 days post-bleomycin treatment (Figure 4D). In the *Acta2-CreERT2; Adra1d*$^{f/f}$ mice that received tamoxifen injections, there was a significant reduction in total lung collagen content, approximately 44%, compared to control mice that received corn oil (Figure 4E). Trichrome staining corroborated these results (Figure 4F and G). These findings provide compelling *in vivo* evidence that interactions between sympathetic nerves and alveolar myofibroblasts can promote lung fibrosis through a functional axis involving noradrenaline and ADRA1D.

In contrast, *Acta2-CreERT2; Adra1d*$^{f/f}$ mice that received tamoxifen timed to delete ADRA1D before bleomycin administration (Figure S3A) showed no improvement in collagen measurements compared to their corn-oil treated littermates (Figures S3B). These findings suggest that pulmonary fibrosis mediated by noradrenergic interactions between sympathetic nerves and myofibroblasts is unlikely to involve an ADRA1D+ α-SMA+ cell present at the time of injury.

Adra1d deletion in myeloid cells is dispensable for fibrosis

Given that ADRA1D+ macrophages were also increased following injury (Figure S4), we also evaluated a contribution of these fibrogenic myeloid cells in the *LysMCre; Adra1d*$^{f/f}$ mouse line. The *LysMCre* promoter is active in all cells of myeloid lineage, along with a small proportion of

lung epithelia, and has been previously used in pulmonary fibrosis studies [42]. In our work, the crossing of *LysMCre* mice with the *Adra1d*$^{f/f}$ mouse line achieved isotype specific deletion in macrophages without off target deletion in epithelium (Figures S5A-C, Figure S6). We treated *LysMCre; Adra1d*$^{f/f}$ mice with bleomycin and observed that deleting ADRA1D in this manner did not affect collagen content (Figure S5D) or trichrome staining (Figures S5E-H) 14 days post-injury. These findings suggest that ADRA1D's involvement in pathological lung remodeling is likely independent of its expression in *LysMCre*+ myeloid cells, and point to a sympathetic nerve-myofibroblast axis in this form of noradrenaline-mediated pulmonary fibrosis.

Noradrenaline stimulates expansion of human lung myofibroblasts via an α1-adrenoreceptor dependent, cell autonomous mechanism

Finally, to complete the description of a functional axis comprised of noradrenaline, α1-ARs, and fibroblasts, we sought information that can only be obtained via the reductionist methods of cell culture. In experiments with MRC5 human lung fibroblasts, noradrenaline treatment induced a state of α1-AR dependent cell proliferation (Figures 5A-E). These observations were further corroborated when 3-(4,5-Dimethylthiazol-2-yl)-2,5-diphenyltetrazolium bromide (MTT) assays revealed a decrease in MTT signals in both MRC5 and IPF lung fibroblasts, but not NHLFs, following terazosin treatment (Figure 5F).

Further analysis revealed the direct involvement of α1-ARs, specifically ADRA1D, in human lung fibrogenesis. This was demonstrated using human precision-cut lung slices. Exposure to a fibrotic cocktail triggered α-SMA (ACTA2) expression in stromal cells adjacent to alveoli, with some cells showing ADRA1D co-expression. This pattern correlated with the fibrotic histology observed in the lungs (Figures 5G-I) and was consistent with *ACTA2* expression measured by PCR analysis (Figure 5J). Importantly, the addition of terazosin to the culture media reversed these effects (Figures 5G-J). These results underscore the critical function of α1-ARs,

417 particularly ADRA1D, in driving fibrotic pathologies through a cell-autonomous mechanism in
418 fibroblasts (Figure 6).

419

420 **DISCUSSION**

421 The discovery that sympathetic nerves direct pulmonary fibrosis by innervating myofibroblasts
422 provides fundamental new insights into the repair and pathologic remodeling of injured organs.
423 Our work puts forth compelling evidence that sympathetic innervation controls noradrenergic
424 fibrotic remodeling and illuminates new concepts in tissue repair. These discoveries include the
425 functional benefit enacted by direct loss of sympathetic nerves and pharmacologic interruption
426 of noradrenaline's neurotransmitter receptors, and the evidence of functional noradrenergic
427 input from sympathetic nerves to ADRA1D+ myofibroblasts in well accepted mouse models,
428 advanced lung mimetics, and several fibrotic conditions affecting human lungs. Given the lung's
429 dependence on innervation for proper development and functional homeostasis [22], we predict
430 that this newly described nerve-fibroblast axis controls numerous aspects of lung physiology in
431 health and disease. Furthermore, considering the pivotal and highly conserved nature of
432 sympathetic innervation, noradrenaline, and myofibroblasts across tissues, we predict that this
433 axis contributes to homeostasis, repair, and pathologic remodeling in numerous organs.

434 The discovery of a functional axis involving sympathetic nerves and fibrogenic myofibroblasts
435 augments the nascent field of nerve-lung interactions in the adult mammals. In recent years the
436 availability of advanced imaging methods [43], genetic tools [44], and single cell sequencing [45],
437 has facilitated studies of autonomic and/or sensory innervation as contributors to lung pathology.
438 Much of this work provided indirect evidence, and none studied myofibroblast innervation in
439 alveolar repair and fibrosis. Therefore, our finding that sympathetic nerves are absolutely
440 required for maximal fibrosis provides first of its kind insights to lung biology that raise numerous

questions that warrant further study. For example, the nature of nerve endings has yet to be determined, so it is not clear whether sympathetic nerve derived neurotransmitters such as noradrenaline reach their target through free nerve endings, diffusion, or alternate mechanisms [46]. Additionally, direct sympathetic denervation only partially mitigated fibrosis, which could reflect non-adrenergic nerve functions or compensatory mechanisms such as denervation hypersensitivity [47]. Since Cre drivers and pharmacological interventions are not lung-specific, we cannot discount the possibility of contributions from mechanisms occurring in peripheral organs or the central nervous system. Rather than undermining our findings, this latter possibility bolsters the exciting concept of systemic control of tissue level responses and provides an urgent mandate for additional study of this intriguing new paradigm.

Our study provides definitive evidence of a new fibrotic pathway involving sympathetic nerves and myofibroblasts, the mechanism of which is currently unknown. The benefit was observed only when *Adra1d* deletion occurred in myofibroblasts during fibrogenesis, suggesting that the mechanism does not involve the expansion of an ADRA1D+ α-SMA+ progenitor population. Instead, it appears to be an effect on fibrogenesis mediated by an emerging population of ADRA1D+ myofibroblasts. As shown by our *ex vivo* studies, this process is likely at least partially due to sympathetic innervation-induced alterations in such fundamental cell fate decisions of proliferation and survival. Of course, we cannot rule out a contribution of additional mechanisms such as regression to a state of phenotypic quiescence. Additionally, although our findings provide clear evidence that myofibroblasts are a primary recipient of cues from sympathetic nerves, we cannot exclude the possibility of non-cell-autonomous mechanisms. In fact, the widespread expression of receptors for sympathetic nerve derived neurotransmitters makes such a possibility highly likely and provides numerous new avenues for investigative studies aimed at mechanistic discovery. Finally, the existence of numerous pharmacologic

agents targeting noradrenergic GPCRs and the emergence of clinical strategies based on targeted neuromodulation [48] leave us well positioned for therapeutic breakthroughs.

In conclusion, we provide evidence of a functional axis involving sympathetic nerves and myofibroblasts in pulmonary fibrosis. This discovery provides new insight into how cells send and receive signals in the adult lung. It also provides new insight into how nerves communicate with tissues during conditions of injury and regenerative failure. It shows how two distinct organs – autonomic nerves and the lung – interact during fibrogenesis in adult mammals. Last, it provides proof of concept evidence for the development of neuromodulation-based strategies to treat myofibroblast driven conditions in humans. Further study of these important areas will illuminate paradigm shifting discoveries in tissue repair.

ACKNOWLEDGEMENTS

We would like to express our gratitude to Ruijuan Gao at the Chinese Academy of Medical Sciences and Peking Union Medical College for providing several of the immunofluorescence images featured in our manuscript. We also extend our heartfelt thanks to all the patients living with fibrotic lung disease. Your strength, courage, and resilience deeply inspire us and fuel our commitment to advancing research in this field.

COMPETING INTERESTS

The authors declare that there is no conflict of interest.

DATA AVAILABILITY

The data that support the findings of this study are available on request from the corresponding author.

FIGURE LEGENDS

Figure 1: Noradrenergic signals and sympathetic nerves contribute to pulmonary fibrosis (A-E) Wild-type mice were administered 2.0 U/kg orotracheal bleomycin or control vehicle on Day 0 and sacrificed on Day 14. Bleomycin challenge resulted in increased collagen deposition, as evidenced by trichrome staining (A, B) and elevated right lung collagen content (C, $P < 0.0001$). BAL noradrenaline levels were significantly increased following bleomycin administration (D, $P = 0.0138$), while plasma levels remained unchanged (E). (F-K) Immunofluorescence and confocal imaging revealed α-SMA (red), PGP9.5 or TH (green), and

DAPI nuclear staining (blue) in mouse lungs treated with vehicle or bleomycin. Normal lungs showed typical expression of PGP9.5 and TH in airways and blood vessels (F, I). Fibrotic lungs retained these markers and also displayed PGP9.5 or TH-positive nerves in alveolar regions (G, J). A significant positive correlation was established between both nerve types and these key effector cells (P = 0.0134 and P = 0.0203, respectively). (L-O) Mice with genetic deletion of TrkA in sympathetic nerves (genotype: *Th-Cre; Ntrk1*$^{f/f}$) or intact TrkA (*Th-Cre*) were given orotracheal bleomycin on Day 0 and sacrificed on Day 14. In *Th-Cre; Ntrk1*$^{f/f}$ mice, BAL noradrenaline levels were reduced (L, P = 0.0267), along with decreased right lung collagen content (M, P = 0.0491) and improved trichrome staining (N, O). Images were captured at 20x magnification. Data are presented as mean ± SEM or median ± IQR. Statistical comparisons were conducted using Student's t-test for normally distributed data and Mann-Whitney test for non-normally distributed data. Statistical correlations were conducted using Spearman's Rank Correlation Coefficient. *P < 0.05, ****P < 0.0001. α-SMA, alpha-smooth muscle actin; BAL, bronchoalveolar lavage; DAPI, 4',6-diamidino-2-phenylindole; HPF, high-power field; PGP9.5, ubiquitin carboxy-terminal hydrolase L1; TH, tyrosine hydroxylase.

Figure 2: Noradrenaline-driven fibrogenesis requires functional neurotransmitter receptors. (A-D) Wild-type mice received orally administered terazosin, an α1-adrenoceptor antagonist, at 1 or 10 mg/kg, or a vehicle from Days 5 to 13 post-bleomycin challenge and were euthanized on Day 14. Terazosin dosed at 1 mg/kg reduced collagen accumulation (A, P = 0.0291) and trichome staining (B--D). (E-H) Treatment with atenolol, a β1-adrenoceptor antagonist, and ICI118,551, a β2-adrenoceptor antagonist, at 1 mg/kg intraperitoneally improved both collagen deposition (E, P = 0.0021; P = 0.0098, respectively) and trichrome staining (F-H). (I-L) Intraperitoneal injections of nisoxetine, a NAT antagonist, at 3 or 10 mg/kg did not reduce collagen accumulation (I) or improve trichrome staining (J-L). (M-O) Both wild-type (*Slc6a2*$^{+/+}$) and NAT-deficient (*Slc6a2*$^{-/-}$) mice were subjected to inhaled bleomycin without observing any protective effect against collagen accumulation in NAT-deficient mice (M) or improvement in trichrome staining (N, O). Images were captured at 20x magnification. Data are presented as mean ± SEM or median ± IQR. Statistical analyses were conducted using Student's t-test or ANOVA with Tukey's multiple comparisons for normally distributed data, and Kruskal-Wallis tests with Dunn's multiple comparisons for non-normally distributed data. *P < 0.05, **P < 0.01. NAT, noradrenaline transporter; Slc6a2, solute carrier family 6 member 2.

Figure 3: Fibrotic lungs contain α1-adrenoreceptor-expressing myofibroblasts. (A-D) Representative immunofluorescence imaging of mouse lung tissues at day 14 post-bleomycin treatment (A, B) showed α-SMA (red), ADRA1D (green), and DAPI (blue) cells. A marked increase in ADRA1D-expressing myofibroblasts (white arrows) was observed in bleomycin-treated mice. (C, D) Flow cytometric analysis of wild-type mice post-orotracheal bleomycin administration, with ADRA1D expression in α-SMA-positive cells peaking on day 14 (D, P = 0.0026). (E-L) Immunofluorescence imaging revealed ADRA1D expression (red), α-SMA (green), and nuclear staining with DAPI (blue) in lung explant tissues from IPF, SSc-ILD, and normal lung tissues. (E-G) Normal lung tissues exhibited ADRA1D expression in luminal structures such as airways and blood vessels (E, white arrows), as well as in scattered cells throughout the alveoli (E, white asterisks). Similar patterns were observed in IPF and SSc-ILD tissues, with additional ADRA1D-positive cells in fibrotic areas, resembling cells of inflammatory or stromal lineage (white asterisks and white hashtags, respectively, F, G). The prevalence of ADRA1D-expressing cells was significantly higher in IPF and SSc-ILD tissues than in normal lungs (H, P = 0.0306 and P = 0.0398, respectively). (I-L) Compared to normal lung tissues, a

higher accumulation of cells co-expressing ADRA1D and α-SMA (white arrows) was observed in IPF and SSc-ILD tissues (L, $P = 0.0003$ and $P = 0.0296$, respectively). Images were captured at 20x magnification. Data are presented as mean ± SEM, and statistical analyses were conducted using Student's t-test. *$P < 0.05$, **$P < 0.01$, ***$P < 0.001$. ADRA1D, α1-adrenoreceptor subtype D; α-SMA, alpha-smooth muscle actin; DAPI, 4′,6-diamidino-2-phenylindole; HPF, high-power field; IPF, idiopathic pulmonary fibrosis; SSc-ILD, systemic sclerosis-related interstitial lung disease.

Figure 4: Conditional deletion of ADRA1D in myofibroblasts attenuates fibrosis. Utilizing a myofibroblast-specific knockout approach, *Acta2-CreERT2* mice were crossed with *Adra1d*$^{f/f}$ mice (A) to produce *Acta2-CreERT2; Adra1d*$^{f/f}$ offspring. (B, C) A targeted reduction in *Adra1d* expression within Zs+ (ACTA2+) cells (C, $P = 0.0150$). (D) *Acta2-CreERT2; Adra1d*$^{f/f}$ mice received tamoxifen or vehicle timed to delete ADRA1D 7 days after bleomycin administration. (E-G) Specific deletion of ADRA1D in α-SMA-expressing cells results in reduced collagen deposition (E, $P = 0.0024$) and improved trichrome staining (F, G). Images were captured at 20x magnification. Data are presented as mean ± SEM or median ± IQR, with statistical tests including Student's t-test for normally distributed data and Mann-Whitney for non-normally distributed data. *$P < 0.01$, **$P < 0.01$. ADRA1D, α1-adrenoreceptor subtype D; α-SMA, alpha-smooth muscle actin; TAM, tamoxifen; Zs, ZsGreen.

Figure 5: α1-adrenergic antagonism modulates fibroblast proliferation and attenuates fibrosis in human lung models. (A-D) Immunofluorescence imaging displayed BrdU (green) and nuclear staining with propidium iodide (PI) (red) in MRC5 human lung fibroblasts. A dose-dependent increase in BrdU incorporation was observed in MRC5 cells stimulated with increasing concentrations of noradrenaline (NA), peaking at 25 μM (D, $P = 0.0159$). This response was reversed upon co-incubation with terazosin (E, $P = 0.0441$). (F) MTT assays demonstrated a significant reduction in the number of viable cells in MRC5 human lung fibroblasts and IPF fibroblasts when stimulated with NA and treated with terazosin ($P = 0.0493$ and $P = 0.0156$, respectively). This effect was not observed in normal human lung fibroblasts, indicating that IPF fibroblasts are poised to receive and respond to noradrenergic signals via an α1-AR dependent mechanism. (G-I) Immunofluorescence imaging demonstrated expression of ADRA1D (red) and α-SMA (green), with nuclear staining by DAPI (blue) in human precision-cut lung slices. Following exposure to a fibrotic cocktail, a marked increase in α-SMA (ACTA2) expression was observed in stromal cells adjacent to alveoli, with some cells showing co-expression of ADRA1D (white arrows, G, H). This expression pattern was consistent with trichrome staining and matched *ACTA2* expression quantified by PCR analysis (J, $P = 0.0236$). The introduction of terazosin to the culture media reversed these fibrotic effects (I, J, $P = 0.0106$). Images were captured at 20x magnification. Data are presented as mean ± SEM or median ± IQR, with statistical analysis performed using Student's t-test for normally distributed data and Mann-Whitney or Kruskal-Wallis tests with Dunn's multiple comparisons for non-normally distributed data. *$P < 0.05$, **$P < 0.01$. ADRA1D, α1-adrenoreceptor subtype D; α-SMA, alpha-smooth muscle actin; BrdU, bromodeoxyuridine; DAPI, 4′,6-diamidino-2-phenylindole; FC, fibrotic cocktail; IPF, idiopathic pulmonary fibrosis; MTT, 3-(4,5-Dimethylthiazol-2-yl)-2,5-diphenyltetrazolium bromide; NA, noradrenaline; NHLF, normal human lung fibroblast; PCR, polymerase chain reaction; PI, propidium iodide; TZ, terazosin.

Figure 6: A nerve-fibroblast axis in pulmonary fibrosis. Following alveolar injury, sympathetic nerves stimulate noradrenaline-mediated myofibroblast accumulation via an

ADRA1D-dependent, cell autonomous mechanism. ADRA1D, α1-adrenoreceptor subtype D; NA, noradrenaline. The figure was created using BioRender.com.

REFERENCES

1. Raghu, G., et al., *An official ATS/ERS/JRS/ALAT statement: idiopathic pulmonary fibrosis: evidence-based guidelines for diagnosis and management.* Am J Respir Crit Care Med, 2011. **183**(6): p. 788-824.
2. Travers, J.G., et al., *Cardiac Fibrosis: The Fibroblast Awakens.* Circ Res, 2016. **118**(6): p. 1021-40.
3. Berumen, J., et al., *Liver fibrosis: Pathophysiology and clinical implications.* WIREs Mech Dis, 2021. **13**(1): p. e1499.
4. Huang, R., P. Fu, and L. Ma, *Kidney fibrosis: from mechanisms to therapeutic medicines.* Signal Transduct Target Ther, 2023. **8**(1): p. 129.
5. Shaw, T.J., K. Kishi, and R. Mori, *Wound-associated skin fibrosis: mechanisms and treatments based on modulating the inflammatory response.* Endocr Metab Immune Disord Drug Targets, 2010. **10**(4): p. 320-30.
6. Henderson, N.C., F. Rieder, and T.A. Wynn, *Fibrosis: from mechanisms to medicines.* Nature, 2020. **587**(7835): p. 555-566.
7. King, T.E., Jr., et al., *A phase 3 trial of pirfenidone in patients with idiopathic pulmonary fibrosis.* N Engl J Med, 2014. **370**(22): p. 2083-92.
8. Richeldi, L., et al., *Efficacy and safety of nintedanib in idiopathic pulmonary fibrosis.* N Engl J Med, 2014. **370**(22): p. 2071-82.
9. Tsukui, T., P.J. Wolters, and D. Sheppard, *Alveolar fibroblast lineage orchestrates lung inflammation and fibrosis.* Nature, 2024. **631**(8021): p. 627-634.
10. Younesi, F.S., et al., *Fibroblast and myofibroblast activation in normal tissue repair and fibrosis.* Nat Rev Mol Cell Biol, 2024. **25**(8): p. 617-638.
11. Roman, J., *Fibroblasts-Warriors at the Intersection of Wound Healing and Disrepair.* Biomolecules, 2023. **13**(6).
12. Ishikawa, G., et al., *alpha1 Adrenoreceptor antagonism mitigates extracellular mitochondrial DNA accumulation in lung fibrosis models and in patients with idiopathic pulmonary fibrosis.* Am J Physiol Lung Cell Mol Physiol, 2023. **324**(5): p. L639-L651.
13. Xue, J., et al., *Impact of Liver Sympathetic Nervous System on Liver Fibrosis and Regeneration After Bile Duct Ligation in Rats.* J Mol Neurosci, 2024. **74**(1): p. 4.
14. Gao, R., et al., *Macrophage-derived netrin-1 drives adrenergic nerve-associated lung fibrosis.* J Clin Invest, 2021. **131**(1).
15. Sigala, B., et al., *Sympathetic nervous system catecholamines and neuropeptide Y neurotransmitters are upregulated in human NAFLD and modulate the fibrogenic function of hepatic stellate cells.* PLoS One, 2013. **8**(9): p. e72928.
16. Borovac, J.A., et al., *Sympathetic nervous system activation and heart failure: Current state of evidence and the pathophysiology in the light of novel biomarkers.* World J Cardiol, 2020. **12**(8): p. 373-408.
17. Levick, S.P., et al., *Sympathetic nervous system modulation of inflammation and remodeling in the hypertensive heart.* Hypertension, 2010. **55**(2): p. 270-6.
18. Li, Q., et al., *Sympathetic Denervation Ameliorates Renal Fibrosis via Inhibition of Cellular Senescence.* Front Immunol, 2021. **12**: p. 823935.
19. Pongratz, G. and R.H. Straub, *The sympathetic nervous response in inflammation.* Arthritis Res Ther, 2014. **16**(6): p. 504.

20. Ulloa, L., S. Quiroz-Gonzalez, and R. Torres-Rosas, *Nerve Stimulation: Immunomodulation and Control of Inflammation.* Trends Mol Med, 2017. **23**(12): p. 1103-1120.
21. Gorji, A., *Neuroinflammation: The Pathogenic Mechanism of Neurological Disorders.* Int J Mol Sci, 2022. **23**(10).
22. Zhang, K., et al., *A functional circuit formed by the autonomic nerves and myofibroblasts controls mammalian alveolar formation for gas exchange.* Dev Cell, 2022. **57**(13): p. 1566-1581 e7.
23. *Guide for the Care and Use of Laboratory Animals, 8th edition*. 2011: Washington (DC).
24. Zhou, Y., et al., *Chitinase 3-like 1 suppresses injury and promotes fibroproliferative responses in Mammalian lung fibrosis.* Sci Transl Med, 2014. **6**(240): p. 240ra76.
25. Sheikh, A.Q., et al., *Cell Autonomous and Non-cell Autonomous Regulation of SMC Progenitors in Pulmonary Hypertension.* Cell Rep, 2018. **23**(4): p. 1152-1165.
26. Izbicki, G., et al., *Time course of bleomycin-induced lung fibrosis.* Int J Exp Pathol, 2002. **83**(3): p. 111-9.
27. Jiang, H., et al., *Dense Intra-adipose Sympathetic Arborizations Are Essential for Cold-Induced Beiging of Mouse White Adipose Tissue.* Cell Metab, 2017. **26**(4): p. 686-692 e3.
28. Aloe, L., et al., *Nerve Growth Factor: A Focus on Neuroscience and Therapy.* Curr Neuropharmacol, 2015. **13**(3): p. 294-303.
29. Liu, P., S. Li, and L. Tang, *Nerve Growth Factor: A Potential Therapeutic Target for Lung Diseases.* Int J Mol Sci, 2021. **22**(17).
30. Rubin, L., et al., *Neurotrophic factors and their receptors in lung development and implications in lung diseases.* Cytokine Growth Factor Rev, 2021. **59**: p. 84-94.
31. Tortorolo, L., et al., *Neurotrophin overexpression in lower airways of infants with respiratory syncytial virus infection.* Am J Respir Crit Care Med, 2005. **172**(2): p. 233-7.
32. Bonisch, H. and M. Bruss, *The norepinephrine transporter in physiology and disease.* Handb Exp Pharmacol, 2006(175): p. 485-524.
33. Pramod, A.B., et al., *SLC6 transporters: structure, function, regulation, disease association and therapeutics.* Mol Aspects Med, 2013. **34**(2-3): p. 197-219.
34. Koenecke, A., et al., *Alpha-1 adrenergic receptor antagonists to prevent hyperinflammation and death from lower respiratory tract infection.* Elife, 2021. **10**.
35. Rose, L., et al., *The Association Between Alpha-1 Adrenergic Receptor Antagonists and In-Hospital Mortality From COVID-19.* Front Med (Lausanne), 2021. **8**: p. 637647.
36. Weber, M.A., et al., *Glycolysis-enhancing alpha(1)-adrenergic antagonists modify cognitive symptoms related to Parkinson's disease.* NPJ Parkinsons Dis, 2023. **9**(1): p. 32.
37. Huan, H.B., et al., *Sympathetic nervous system promotes hepatocarcinogenesis by modulating inflammation through activation of alpha1-adrenergic receptors of Kupffer cells.* Brain Behav Immun, 2017. **59**: p. 118-134.
38. Perez, D.M., *alpha(1)-Adrenergic Receptors: Insights into Potential Therapeutic Opportunities for COVID-19, Heart Failure, and Alzheimer's Disease.* Int J Mol Sci, 2023. **24**(4).
39. El Agha, E., et al., *Two-Way Conversion between Lipogenic and Myogenic Fibroblastic Phenotypes Marks the Progression and Resolution of Lung Fibrosis.* Cell Stem Cell, 2017. **20**(2): p. 261-273 e3.
40. Chakraborty, R., et al., *Promoters to Study Vascular Smooth Muscle.* Arterioscler Thromb Vasc Biol, 2019. **39**(4): p. 603-612.
41. Das, S., et al., *Colonic healing requires Wnt produced by epithelium as well as Tagln+ and Acta2+ stromal cells.* Development, 2022. **149**(1).
42. Misharin, A.V., et al., *Monocyte-derived alveolar macrophages drive lung fibrosis and persist in the lung over the life span.* J Exp Med, 2017. **214**(8): p. 2387-2404.

685 43. Liu, T., et al., *Local sympathetic innervations modulate the lung innate immune*
686 *responses.* Sci Adv, 2020. **6**(20): p. eaay1497.
687 44. Navabpour, S., J.L. Kwapis, and T.J. Jarome, *A neuroscientist's guide to transgenic*
688 *mice and other genetic tools.* Neurosci Biobehav Rev, 2020. **108**: p. 732-748.
689 45. Adams, T.S., et al., *Single-cell RNA-seq reveals ectopic and aberrant lung-resident cell*
690 *populations in idiopathic pulmonary fibrosis.* Sci Adv, 2020. **6**(28): p. eaba1983.
691 46. Mohan, A., et al., *Molecular diffusion model of neurotransmitter homeostasis around*
692 *synapses supporting gradients.* Neural Comput, 2011. **23**(4): p. 984-1014.
693 47. Jones, R. and G. Vrbova, *Two factors responsible for the development of denervation*
694 *hypersensitivity.* J Physiol, 1974. **236**(3): p. 517-38.
695 48. Won, S.M., et al., *Emerging Modalities and Implantable Technologies for*
696 *Neuromodulation.* Cell, 2020. **181**(1): p. 115-135.

697

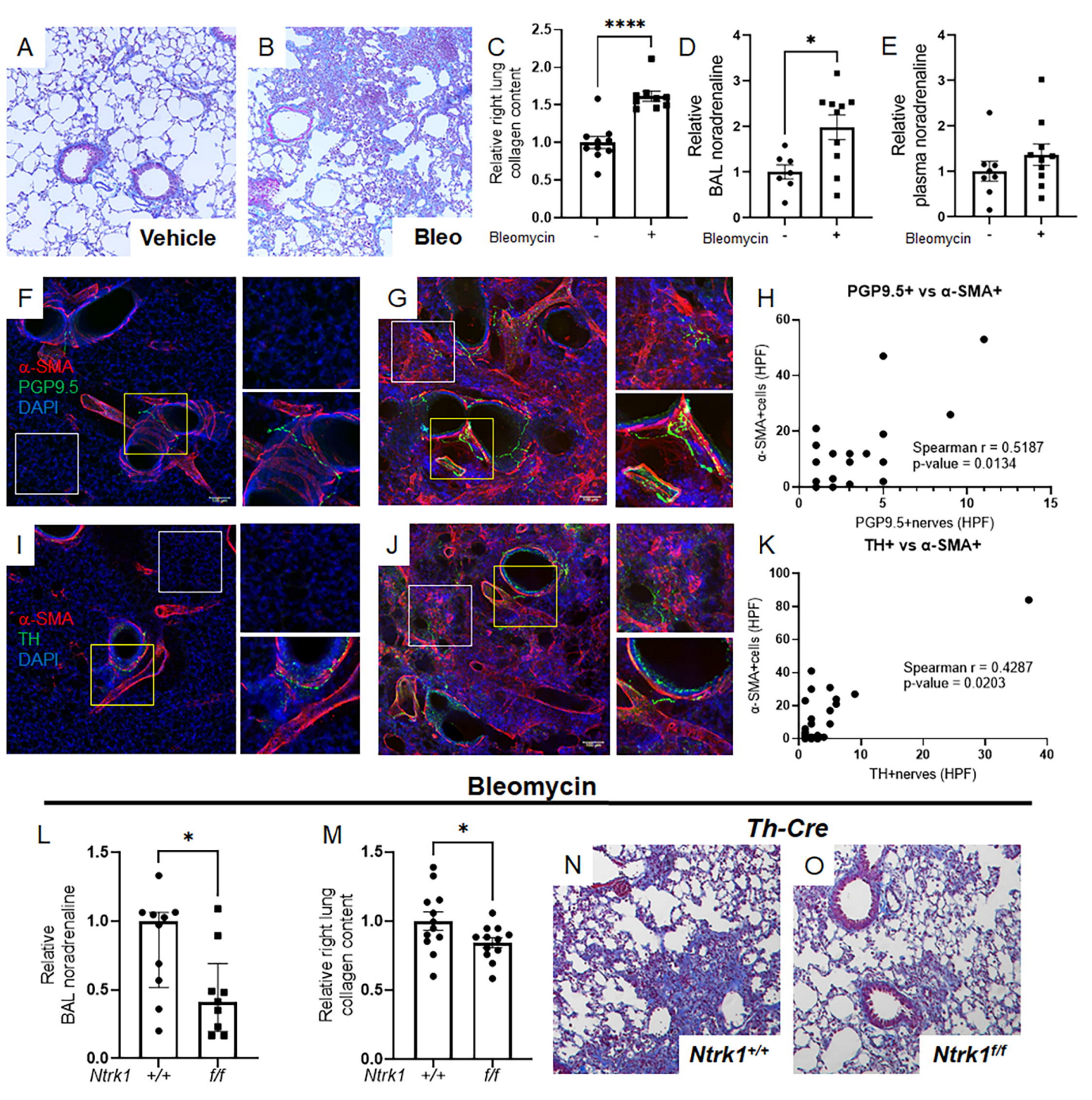
A
Vehicle
B
Bleo
C
Relative right lung collagen content
****
Bleomycin
D
Relative BAL noradrenaline
*
Bleomycin
E
Relative plasma noradrenaline
Bleomycin
F
α-SMA
PGP9.5
DAPI
G
H
PGP9.5+ vs α-SMA+
α-SMA+cells (HPF)
PGP9.5+nerves (HPF)
Spearman r = 0.5187
p-value = 0.0134
I
α-SMA
TH
DAPI
J
K
TH+ vs α-SMA+
α-SMA+cells (HPF)
TH+nerves (HPF)
Spearman r = 0.4287
p-value = 0.0203
Bleomycin
L
Relative BAL noradrenaline
*
Ntrk1 +/+ f/f
M
Relative right lung collagen content
*
Ntrk1 +/+ f/f
Th-Cre
N
Ntrk1+/+
O
Ntrk1f/f

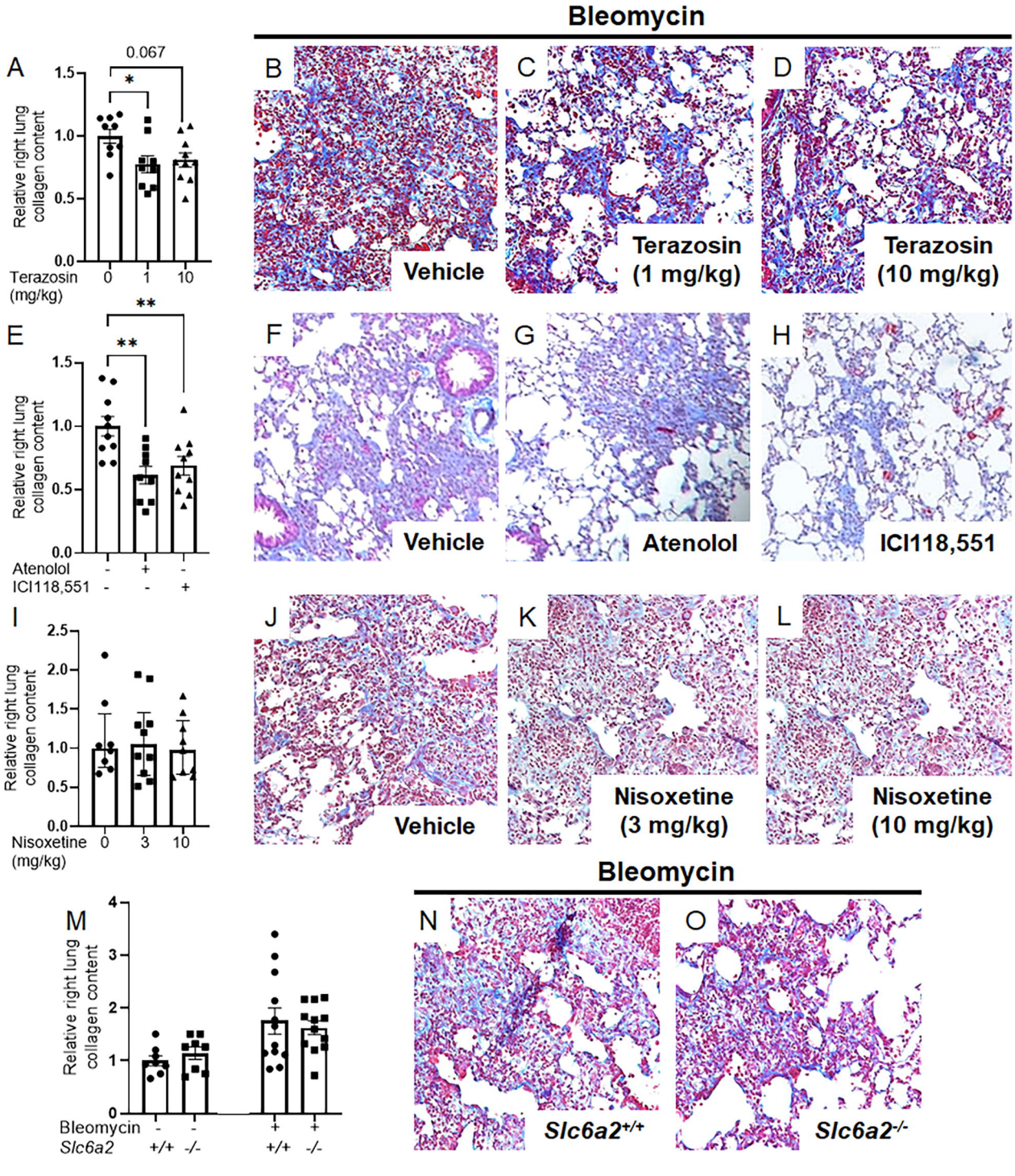
Bleomycin
A
0.067
*
Relative right lung collagen content
1.5
1.0
0.5
0.0
Terazosin (mg/kg)
0
1
10
B
Vehicle
C
Terazosin (1 mg/kg)
D
Terazosin (10 mg/kg)
E
**
**
Relative right lung collagen content
Atenolol
ICI118,551
F
Vehicle
G
Atenolol
H
ICI118,551
I
Relative right lung collagen content
2.5
2.0
1.5
1.0
0.5
0.0
Nisoxetine (mg/kg)
0
3
10
J
Vehicle
K
Nisoxetine (3 mg/kg)
L
Nisoxetine (10 mg/kg)
Bleomycin
M
Relative right lung collagen content
Bleomycin
Slc6a2
+/+
-/-
N
Slc6a2+/+
O
Slc6a2-/-

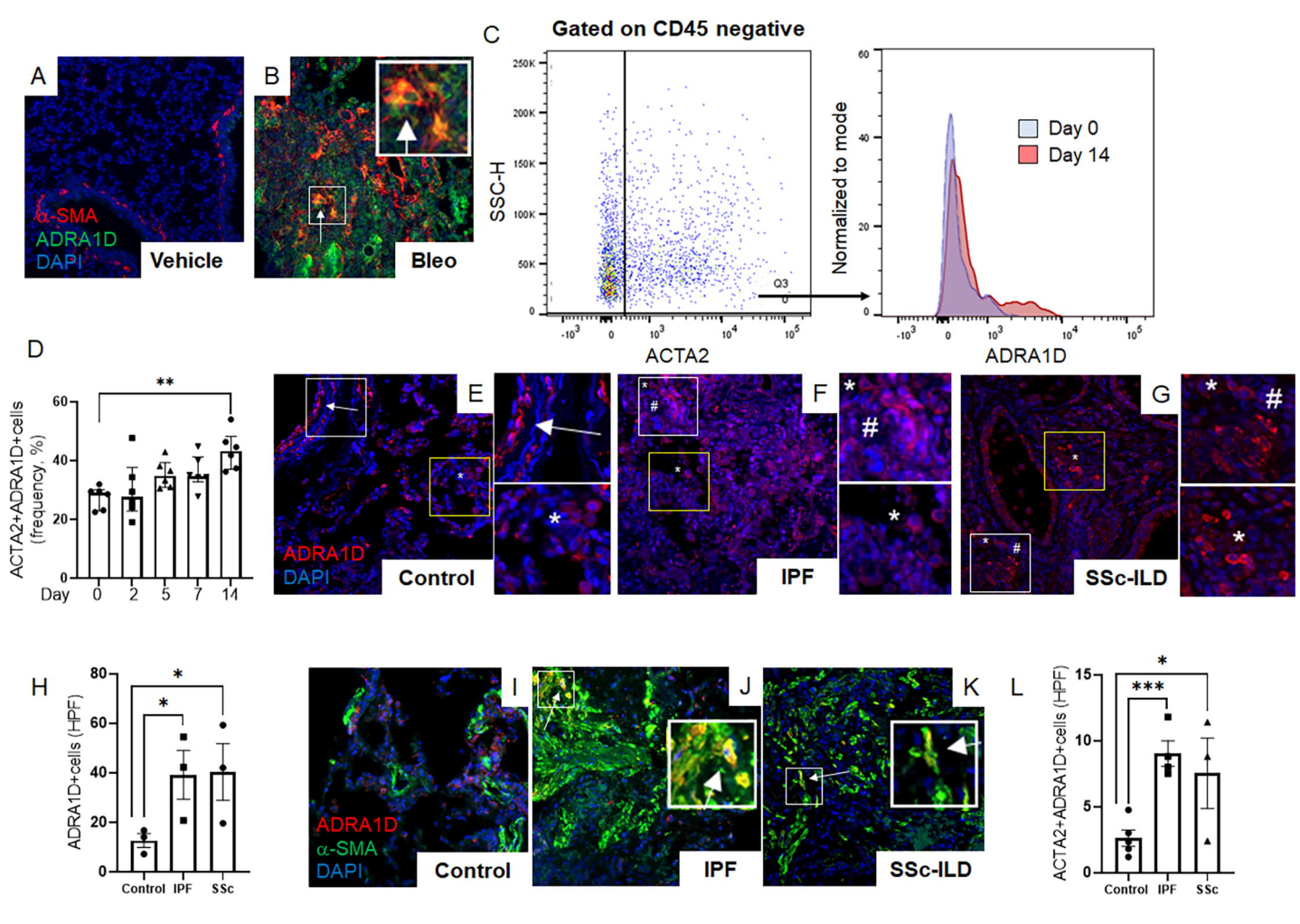
A
α-SMA
ADRA1D
DAPI
Vehicle
B
Bleo
C
Gated on CD45 negative
SSC-H
ACTA2
Q3
Normalized to mode
Day 0
Day 14
ADRA1D
D
ACTA2+ADRA1D+cells (frequency, %)
Day
0
2
5
7
14
**
E
ADRA1D
DAPI
Control
F
IPF
G
SSc-ILD
H
ADRA1D+cells (HPF)
Control
IPF
SSc
*
I
ADRA1D
α-SMA
DAPI
Control
J
IPF
K
SSc-ILD
L
ACTA2+ADRA1D+cells (HPF)
***

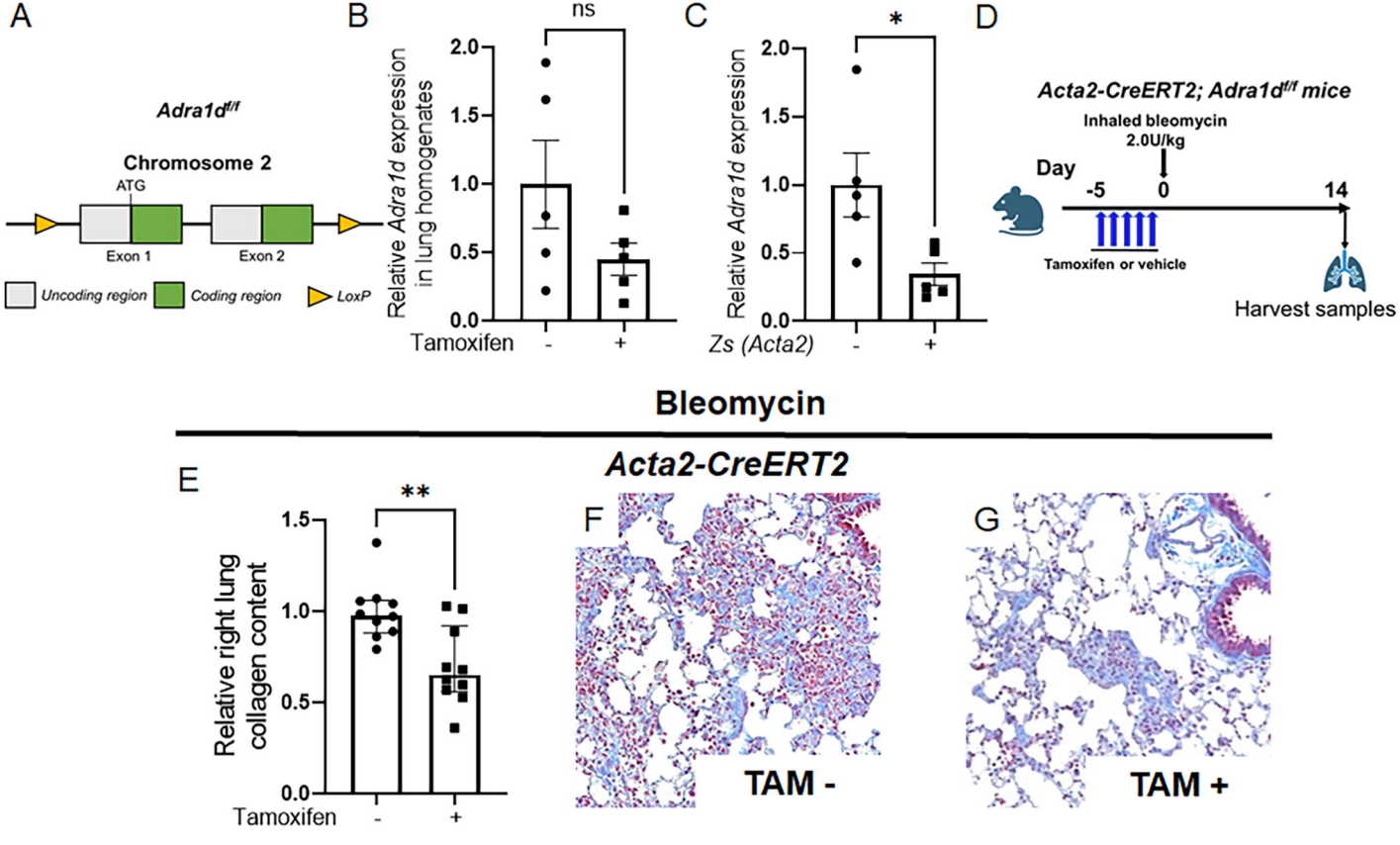
A
Adra1d^f/f
Chromosome 2
ATG
Exon 1
Exon 2
Uncoding region
Coding region
LoxP
B
ns
Relative Adra1d expression in lung homogenates
2.0
1.5
1.0
0.5
0.0
Tamoxifen
-
+
C
*
Relative Adra1d expression
Zs (Acta2)
D
Acta2-CreERT2; Adra1d^f/f mice
Inhaled bleomycin
2.0U/kg
Day
-5
0
14
Tamoxifen or vehicle
Harvest samples
Bleomycin
E
**
Relative right lung collagen content
1.5
1.0
0.5
0.0
Tamoxifen
-
+
Acta2-CreERT2
F
TAM -
G
TAM +

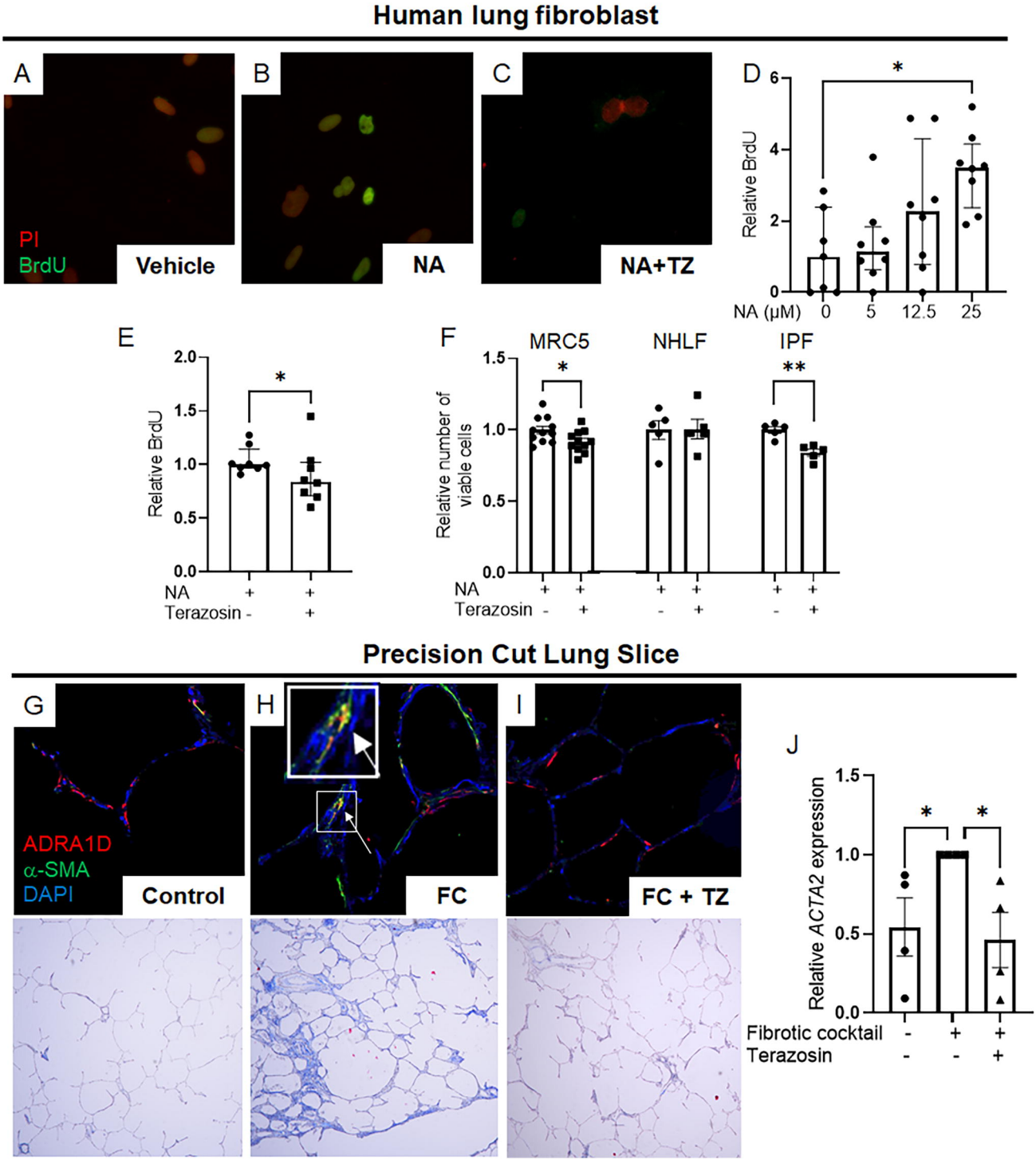
Human lung fibroblast
A
PI
BrdU
Vehicle
B
NA
C
NA+TZ
D
Relative BrdU
NA (μM) 0 5 12.5 25
E
Relative BrdU
NA
Terazosin
F
MRC5
NHLF
IPF
Relative number of viable cells
NA
Terazosin
Precision Cut Lung Slice
G
ADRA1D
α-SMA
DAPI
Control
H
FC
I
FC + TZ
J
Relative ACTA2 expression
Fibrotic cocktail
Terazosin

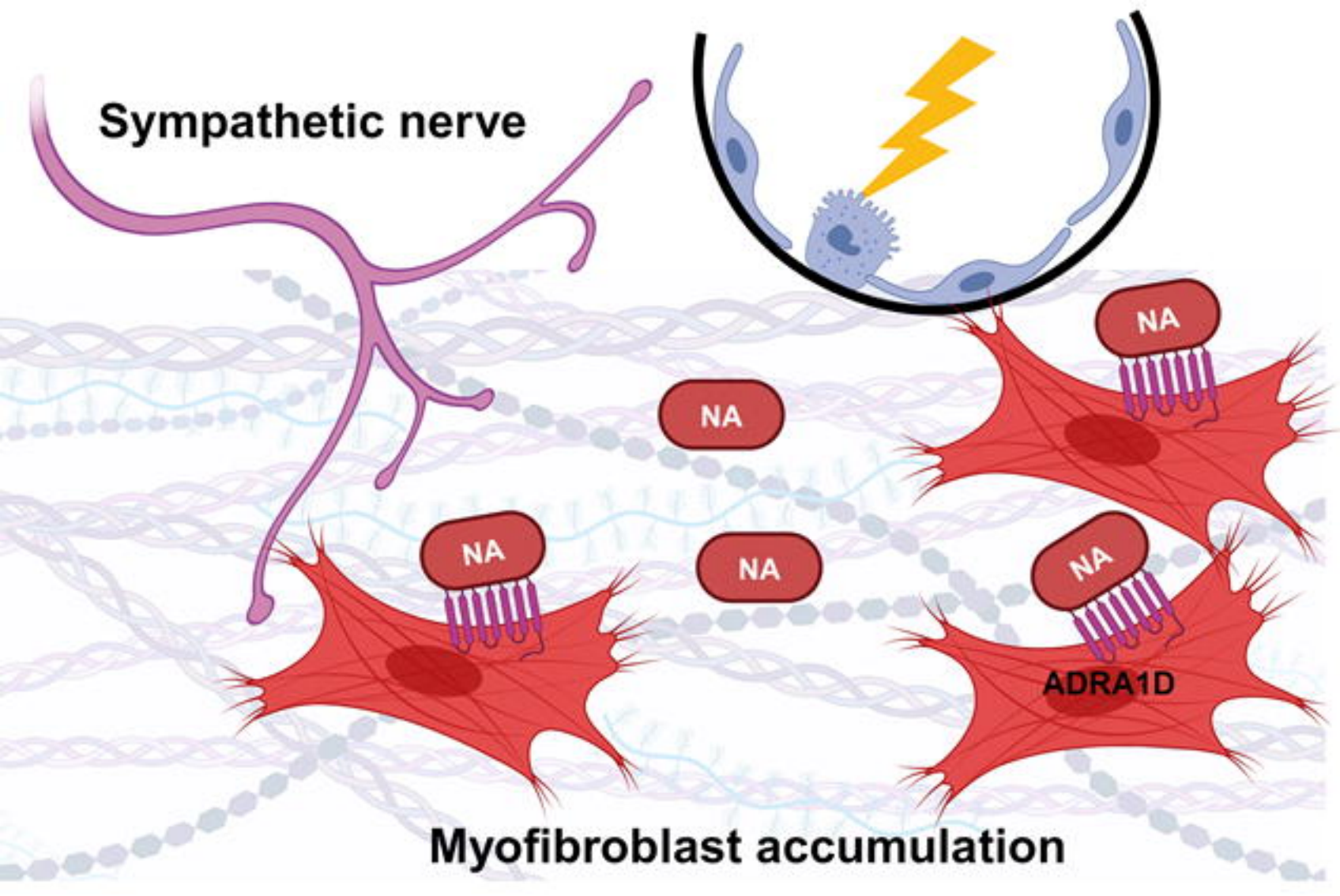
Sympathetic nerve
NA
NA
NA
NA
NA
ADRA1D
Myofibroblast accumulation